

## Computers and Electronics in Agriculture

### Manuscript Details

<b>Manuscript number</b>	COMPAG_2019_1895_R2
<b>Title</b>	MHW-PD: a robust rice panicles counting algorithm based on deep learning and multi-scale hybrid window
<b>Article type</b>	Research Paper

### Abstract

In-field assessment of rice panicle yields accurately and automatically has been one of the key ways to realize high-throughput rice breeding in the modern smart farming. However, practical rice fields normally consist of many different, often very small sizes of panicles, particularly when large numbers of panicles are captured in the imagery. In these cases, the integrity of panicle feature is difficult to extract due to the limited panicle original information and substantial clutters caused by heavily compacted leaves and stems, which results in poor counting efficacy. In this paper, we propose a simple, yet effective method termed as Multi-Scale Hybrid Window Panicle Detect (MHW-PD), which allows the identification and counting of rice panicles robustly independent of the panicle number (density) in the scene. On the basis of quantifying and analyzing the relationship among the receptive field, the size of input image and the average dimensions of panicles, the MHW-PD gives dynamic strategies for choosing the appropriate feature learning network and constructing adaptive multi-scale hybrid window (MHW), which maximizes the richness of panicle feature. Besides, a fusion algorithm is involved to remove the repeated counting of the broken panicles to get the final panicle number. With extensive experimental results, the MHW-PD has achieved ~87% of panicle counting accuracy; and the counting accuracy just decreases by ~8% when the number of panicles per image increases from 0 to 80, which shows better in stability than all the competing methods adopted in this work. The MHW-PD is demonstrated qualitatively and quantitatively that is able to deal with high density of panicles.

**Keywords** Rice; Panicle counting; Deep learning; Multi-Scale Hybrid window; Faster-RCNN;

**Corresponding Author** Haiyan Jiang

**Corresponding Author's Institution** Nanjing Agricultural University

**Order of Authors** Xu Can, Haiyan Jiang, Peter Yuen, Zaki Zaki, Chen Yao **Corresponding Author's Institution**

### Highlights

- (1) A counting algorithm is developed for in-field rice panicles with high density.
- (2) The appropriate CNN is chosen by analyzing receptive field and panicle size.
- (3) A MHW is calculated quantitatively to maximize the richness of panicle feature.
- (4) A fusion module is involved to remove the repeated counting of broken panicle.
- (5) Stability and robustness of MHW-PD is demonstrated by several experiments.

1 ***MHW-PD: a robust rice panicles counting algorithm based on***  
2 ***deep learning and multi-scale hybrid window***

3 ***Xu Can<sup>1</sup>, Jiang Haiyan<sup>1, 2\*</sup>, Peter Yuen<sup>3</sup>, Zaki Ahmad Khan<sup>1</sup>, Chen Yao<sup>1</sup>***

4 ***1 College of Information science & Technology, Nanjing Agricultural University***

5 ***Nanjing 210095, Jiangsu, China***

6 ***2 National Engineering & Technology Center for Information Agricultural,***

7 ***Nanjing Agricultural University Nanjing 210095, Jiangsu, China***

8 ***3 Electro-Optics & Remote Sensing, Centre for Electronics Warfare, Information &***

9 ***Cyber (CEWIC), Cranfield University, Swindon, U.K***

10 **Abstract**

11 In-field assessment of rice panicle yields accurately and automatically has been one of  
12 the key ways to realize high-throughput rice breeding in the modern smart farming.  
13 However, practical rice fields normally consist of many different, often very small  
14 sizes of panicles, particularly when large numbers of panicles are captured in the  
15 imagery. In these cases, the integrity of panicle feature is difficult to extract due to the  
16 limited panicle original information and substantial clutters caused by heavily  
17 compacted leaves and stems, which results in poor counting efficacy. In this paper, we  
18 propose a simple, yet effective method termed as Multi-Scale Hybrid Window Panicle  
19 Detect (MHW-PD), which focuses on enhance the panicle features to detect and count  
20 the large number of small-sized rice panicles in the in-field scene. On the basis of

21 quantifying and analyzing the relationship among the receptive field, the size of input  
22 image and the average dimensions of panicles, the MHW-PD gives dynamic strategies  
23 for choosing the appropriate feature learning network and constructing adaptive multi-  
24 scale hybrid window (MHW), which maximizes the richness of panicle feature.  
25 Besides, a fusion algorithm is involved to remove the repeated counting of the broken  
26 panicles to get the final panicle number. With extensive experimental results, the  
27 MHW-PD has achieved ~87% of panicle counting accuracy; and the counting  
28 accuracy just decreases by ~8% when the number of panicles per image increases  
29 from 0 to 80, which shows better in stability than all the competing methods adopted  
30 in this work. The MHW-PD is demonstrated qualitatively and quantitatively that is  
31 able to deal with high density of panicles.

32 **Keywords** : Rice; Panicle counting; Deep learning; Multi-Scale Hybrid window;  
33 Faster-RCNN;

## 34 **1 Introduction**

35 The main diet of the population in Asia is predominately rice, thus the monitoring  
36 of rice yield accurately is crucially important to the growers for the prediction of  
37 harvest and the development of strategic growth plan. The yield of cereal crops, such  
38 as rice, is largely determined by three agronomic indicators: the kernel number, the  
39 seed setting rate and the 1000-grain weight(Slafer et al., 2014). Previous researches  
40 (Ferrante et al., 2017; Jin et al., 2017)have shown that the number of kernels per unit  
41 area is the most relevant agronomic traits to grain yield. However, this number of

42 grains per unit area not only relates to the seed setting rate, but also it is strongly  
43 dependent on the number of panicle per unit area. Therefore, it is desirable for the  
44 breeders to obtain the number of panicles per unit area quickly and accurately. At  
45 present, this is often achieved through counting manually in most rice cultivation or  
46 breeding research, which costs huge amount of time and labor. Furthermore, due to  
47 the great morphological similarity between different plants in the field, and also the  
48 subjectivity in individual observers, it is very error-prone for counting rice panicles  
49 manually particularly in large-scale production scenarios. Therefore, a fast and  
50 relatively accurate automatic counting method is needed: for both production as well  
51 as scientific research needs such as phenotyping work.

52 Automatic counting method based on machine vision technology is considered to  
53 be an effective alternative to manual counting, and successful precedents such as the  
54 counting of plant leaves(Aich et al., 2017; Barré et al., 2017; Dobrescu et al., 2017;  
55 Giuffrida et al., 2016) and fruits(Maldonado Jr et al., 2016; Mussadiq et al., 2015;  
56 Stein et al., 2016) have been reported. The effectiveness of this automatic counting  
57 method is heavily dependent on the ability of the machine to recognize the targets. In  
58 terms of automatic counting of rice panicles, the existing panicle recognition methods  
59 can be divided into two main categories: the segmentation technique which bases on  
60 colour and/or textural features and the candidate region-based classification methods.  
61 Panicle segmentation method (Cointault et al., 2008; Pound et al., 2017) extracts the  
62 colour or texture of the panicle, and the rice panicles are segmented from the

63 background before they are counted. Zhou et al. (Zhou et al., 2018) employed  
64 principal component analysis to extract representative features of wheat from RGB  
65 images such as colour, texture and edge for wheat panicle segmentation, and ~80% of  
66 count accuracy by using a trained dual support vector machine has been reported.  
67 Fernandez et al.(Fernandez-Gallego et al., 2018) proposed a fast low-cost wheat  
68 panicle segmentation algorithm which uses Laplacian, Median and Maxima (LMM)  
69 filters to remove clutter backgrounds and had achieved good panicle counting results.  
70 The panicle segmentation method is of a low computational complexity algorithm but  
71 the result is sensitive to the illumination conditions of the imagery data (Guo et al.,  
72 2015).

73 The candidate region classification is the method that clusters features over the  
74 spatial domain. The key of the algorithm is the generation of candidate regions,  
75 through features such as color or texture and the candidate regions are subsequently  
76 formed by using the hysteresis threshold of the I2 color plane (Duan et al., 2015) and  
77 the Laws texture energy over the input image(Qiongyan et al., 2017). This method  
78 eliminates more of the clutter background than that of the segmentation approach,  
79 hence it achieves better counting accuracy to some extents. Alternative approach that  
80 utilizes superpixel technique for improving the quality of the candidate region  
81 generation through better preservation of boundary information and to reduce  
82 boundary adhesions, has been widely explored(Lu et al., 2016). Some authors  
83 employed simple linear iterative clustering for the generation of superpixel and then

84 classified the region candidates using convolutional neural network (Xiong et al.,  
85 2017) or classifier trained based on colour feature(Du et al., 2019). Further study  
86 using more effective segmentation method that utilize superpixel in different scales  
87 and couple with a trained linear regression model for counting different varieties of  
88 rice panicles has also been reported(Olsen et al., 2018).

89       The recent work had made the better use of the powerful feature learning  
90 capabilities of the CNN (Convolutional Neural Network, CNN). More sophisticated  
91 feature learning that utilizes a full convolution network for counting field wheat  
92 spikelet have reported a counting accuracy of about 86%(Alkhudaydi et al., 2019).  
93 Other method(Hasan et al., 2018) used the R-CNN(Girshick et al., 2014) for wheat  
94 panicle identification counting, for the object detection algorithm focus on solving the  
95 composite problem of classification and localization. The latest work(Madec et al.,  
96 2019) introduced the Faster-RCNN(Ren et al., 2015) method into wheat panicle  
97 counting and got a 91% counting accuracy. For the rice panicles we focus on, they  
98 will droop due to their self-weight on the maturity-stage, which means the crowded  
99 panicles cram together with leaves and even occluded by leaves locally. Meanwhile,  
100 the size of the panicles in the image tends to reduce when high density of panicles,  
101 e.g. >50 panicles/image, is captured by the camera. In this case, the very limited  
102 information (color/textural/spatial) of the panicle, which is embedded closely in  
103 substantial amount of clutter background, greatly reduces the feature learning  
104 efficiency of the existing object detection algorithms(He et al., 2015; Liu et al., 2016;

105 Redmon et al., 2016; Redmon et al., 2017) and inevitably resulting in large counting  
106 error. Thus, there is a real need to develop a new auto approach to allow a rapid  
107 counting of the scene with large number of small-sized rice panicles per image.

## 108 **2 Principles and designs of the MHW-PD for panicle counting**

### 109 **2.1 Analysis of application of Faster-RCNN**

110 Faster-RCNN is one of the representative detection algorithms based on  
111 regions(Han et al., 2018), which features the strengths of algorithmic structures like  
112 that of the RCNN(Girshick et al., 2014), the SPP-Net(He et al., 2015) and the Fast-  
113 RCNN (Girshick, 2015). As shown in Figure 1, Faster-RCNN has capabilities such as  
114 feature learning, candidate region generation, target classification and positional  
115 frame generation. When Faster-RCNN learns feature based on a CNN, one important  
116 point is the receptive field, which is defined by the region in the input space that  
117 corresponds to any pixel on a particular CNN's feature map. In the circumstances  
118 when train a model to make classification and location, the receptive field of every  
119 position on the feature map have to span over all the anchors that the target/object  
120 represents. Otherwise the feature vectors of the anchors will not have enough  
121 information to make predictions, leading some objects missed by detection model.  
122 This is particular true when the target in question is relatively small in physical size in  
123 comparison to that of the background objects, for example, the small-sized rice  
124 panicles here in our scenario.

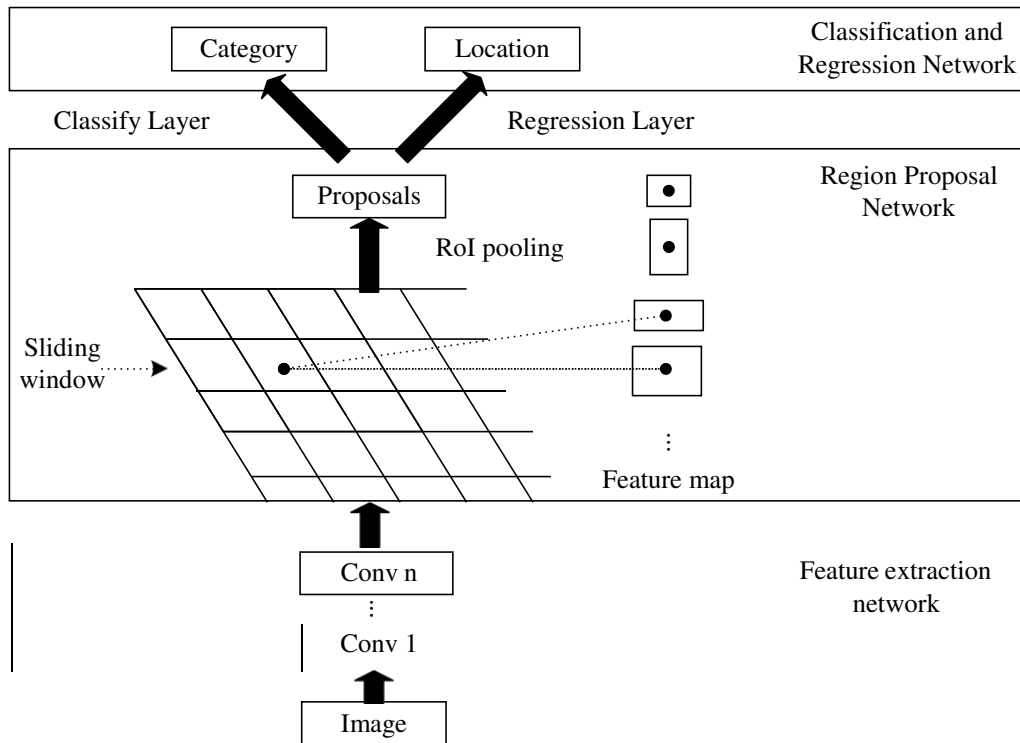


Fig. 1 Outlines the schematic layout of the Faster-RCNN network

## 125 2.2 Overall design of the MHW-PD

126 The objective of the paper is to report an adaptive multi-scale hybrid window  
 127 (MHW) pre-processing technique to enhance the signal to noise ratio of the panicle  
 128 features in the input image, and to couple it with Faster-RCNN network to achieve  
 129 robust counting accuracy for the large number of small-sized panicles in image. For  
 130 the problem of information loss in the process of learning small-sized panicles  
 131 feature, we firstly designed a dynamic mechanism for selecting feature learning  
 132 network, which is based on the relationship between the size of the rice panicle and  
 133 the dimension of the receptive field. Secondly, we dynamically calculated the hybrid  
 134 windows in different scales by partitioning the image into subsections by quantifying  
 135 the relationship between the input image size and the feature learning network



136 parameters. This helps to reduce the background complexity by suppressing the  
 137 clutter background particularly when the number of rice panicles increases. The  
 138 framework of MHW-PD (Figure 2) consists of the following work flow: a) select  
 139 feature learning network dynamically; b) calculate the structure of the hybrid  
 140 windows; c) train the automatic rice panicle counting model based on the Faster-  
 141 RCNN; d) fuse the same rice panicle which has been partitioned into several entities  
 142 to remove the multiple counting; e) output the final number of rice panicles count of  
 143 the test image.

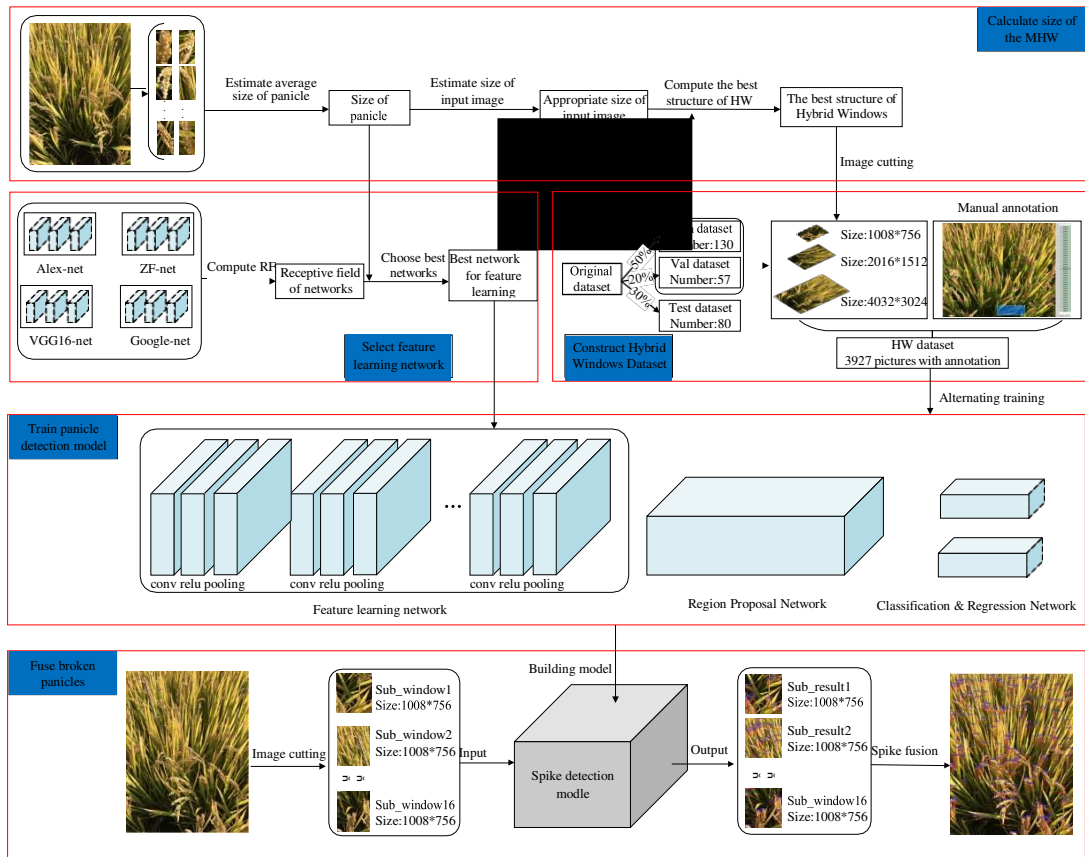


Fig. 2 The schematic layout of the MHW-PD for the robust detection and counting of rice panicles

### 144 2.2.1 Selection of the feature learning network

145 Feature learning is the technique that iteratively abstracts the semantic and  
 146 position information of the target from the image data and converts them into feature

147 maps. The extracted features are dependent on the layer property and thus the  
148 receptive field of a layer can be given by equation (1) (Ren et al., 2018).

$$149 \quad S_R(t) = (S_{RF}(t-1) - 1)N_s(t) + S_f(t) \quad (1)$$

150 Where  $S_{RF}(t)$  and  $N_s(t)$  are the receptive field size and the step size of the  $t^{th}$   
151 convolution layer, and  $S_f(t)$  is the size of filter of the  $t^{th}$  convolution layer. The  
152 ideal dimension of the receptive field is a delicate balance between clutter noise and  
153 the integrity of the extracted feature. In the present Faster-RCNN experiment, the  
154 relationship between the receptive field of the feature learning network and the  
155 object/target has been set as in equation (2):

$$156 \quad \frac{S_{RF}(t)}{S_{obj}(h_{obj}, w_{obj})} \approx 1 \quad (2)$$

157 Where  $S_{obj}(h_{obj}, w_{obj})$  represents the size of the object to be detected, and  $h_{obj}$  and  
158  $w_{obj}$  respectively represent the length and width of the minimum circumscribed  
159 rectangle of the target to be detected. According to equation (2), the ideal dimension  
160 of the receptive field is ideally to be about the same as that of the targets (i.e. the rice  
161 panicles). According to equation (1), the dimensions of the receptive field of the last  
162 convolutional layer of the most popular networks, such as the Alex-Net(Krizhevsky et  
163 al., 2012), ZF-Net(Zeiler et al., 2014), VGG16-Net(Simonyan et al., 2014) and  
164 Google-Net (Szegedy et al., 2015) are tabulated in Table 1. The average sizes (length  
165  $\times$  width) of rice panicles in the image data that have been selected for this work is  
166 about 260 $\times$ 180 pixels. Thus the VGG16 network which features a receptive field of  
167 212 $\times$ 212 may present a closer match to the average panicle dimensions of the data

168 that utilized in this work than other networks. Therefore, the VGG16 network and the  
 169 classification layer have been selected as the feature learning network in this work.

170

**Table 1. Tabulated the receptive field of different nets for the 800×600 pixels input image**

Net name	Reception field of the last layers	$S_{RF}/S_{obj}$
ZF-Net	139×139	0.41
Alex-Net	195×195	0.81
<b>VGG16-Net</b>	<b>212×212</b>	<b>0.96</b>
Google-Net	224×224	1.07

171

### 2.2.2 Design of the Multi-scale Hybrid Window (MHW) Structure

172

Targets are generally regarded as small when they are less than 32×32 pixels or

173

when their length and width are smaller than a tenth of that of the image where they

174

are contained. The construction of a multi-scale hybrid window by partitioning a

175

picture into sub-images will tend to enhance the proportions of the object features

176

with respected to the background within the sub-image, especially when the objects

177

are small. The richer of the target feature will enhance the discrimination ability of the

178

RPN to identify/propose the anchors to be foreground or background thereby

179

improving the detection efficiency. The design of the MHW structure involves the

180

considerations of: i) the various sizes of hybrid windows needed for a given input

181

image, ii) the number of window layers and iii) the selection of layers that are the

182

most suitable to the ranges of various input image sizes.

183

The largest hybrid window that can theoretically be constructed in each layer of

184

the n-layer feature learning network can be given by equation (3):

185

$$\begin{cases} A_H(t) = \frac{H + S(t) + 2 * S_p(t)}{N_s(t)} + 1 \\ A_W(t) = \frac{W + S(t) + 2 * S_p(t)}{N_s(t)} + 1 \end{cases} \quad t = 1, 2, \dots, n \quad (3)$$

186 Where  $A_{H(t)}$  and  $A_{W(t)}$  represent the length and width of the  $t^{th}$  feature map of the  
187 feature learning network respectively,  $H$  and  $W$  represent the length and width of  
188 the original raw image respectively, and  $n$  is maximum number of layers in the  
189 feature learning network.  $N_s(t)$  is the step size of the  $t^{th}$  convolution layer, and  $S_f$   
190 ( $t$ ) is the size of the filter of  $t^{th}$  convolution layer, and  $S_p(t)$  is the expansion of  
191 the  $t^{th}$  convolution layer. The optimal input image size is given in equation (4):

$$192 \quad \begin{cases} h_{in} = \frac{h_{obj}}{T_1} & 0.1 < T_1 < 1 \\ w_{in} = \frac{w_{obj}}{T_2} & 0.1 < T_2 < 1 \end{cases} \quad (4)$$

193 where  $h_{in}$  and  $w_{in}$  represent the length and width of the optimum input image  
194 dimensions;  $h_{obj}$  and  $w_{obj}$  represent the length and width of the smallest rectangle  
195 of the object to be detected respectively;  $T_1$  and  $T_2$  represent the ratio of the length  
196 and width of the object respected to the dimensions of the input image respectively.  
197 The optimal dimensions of the multi-scale hybrid window structure can then be  
198 deduced as shown in equation (5):

$$199 \quad \begin{cases} h_{HW}(i) = A_{H(t)} & A_{H(t)} \in (h_{min}, h_{max}) \\ w_{HW}(i) = A_{W(t)} & A_{W(t)} \in (w_{min}, w_{max}) \end{cases} \quad i = 1, 2, \dots, p \text{ \& } t = 1, 2, \dots, n \quad (5)$$

200 When there are  $p$  layers of multi-scale hybrid windows,  $h_{HW}(i)$  and  $w_{HW}(i)$   
201 represent the optimal length and width of the  $i^{th}$  layer respectively;  $(h_{min}, h_{max})$  and  
202  $(w_{min}, w_{max})$  represent the possible range of the optimal length and width of the input

203 images that will produce the best learning and classification performances.

### 204 **2.2.3 MHW fusion**

205 One of the drawbacks for partitioning the input image into sub-images is the

206 panicle may be unintentionally cut into several parts in different sub-images. To  
 207 eliminate the repeated counting of the same panicle that resides in various sub-images  
 208 during the prediction stage, a fusion algorithm is designed to detect the occurrence of  
 209 the panicle that has been subdivided into parts. A simple way to correct this  
 210 unintentional partition of the target object is to check the vicinity of all the predicted  
 211 boxes. A simple spatial distance monitor algorithm has been implemented to check  
 212 the vicinity of all the predicted location boxes: if two predicted boxes are adjacent or  
 213 very close to each other while their sum of size (height  $\times$  length) is close to the  
 214 average panicle size, e.g. when they are say <10 pixels apart and sum is between  
 215 130 $\times$ 90 pixels and 390 $\times$ 270 pixels (from 1/2 to the 3/2 of the average panicle size),  
 216 the boxes pairs will be merged into one by adopting the largest vertices of the corner  
 217 coordinate as illustrate in Table 2 and Figure 3.

218 **Table 2. The Mini-Code of the Fusion Algorithm for recombining dissected rice panicles**

---

*Input:*  $(x1_n, y1_n, x2_n, y2_n)$ : the coordinates of the left upper and right lower vertices of the panicle detected in sub-windows  
*Output:*  $(x1'_m, y1'_m, x2'_m, y2'_m)$ : the coordinates of prediction boxes fused

*For*( $k = 1; k \leq n; k++$ )  
     *For*( $t = 1; t \leq n; t++$ )  
     *If*( $(|x1_k - x2_t| < 10 \ \&\& \ |y1_k - y2_t| < 2h) \ || \ (|y1_k - y2_t| < 10 \ \&\& \ |x1_k - x2_t| < 2w) \ ||$   
      $(90 < (|y1_k - y2_k| + |y1_t - y2_t|) < 270) \ || \ (130 < (|x1_k - x2_k| + |x1_t - x2_t|) < 390)$   
      $(x1'_m, y1'_m, x2'_m, y2'_m) = (\min(x1_k, x1_t), \min(y1_k, y1_t), \max(x2_k, x2_t), \max(y2_k, y2_t))$   
      $m++;$

---

219

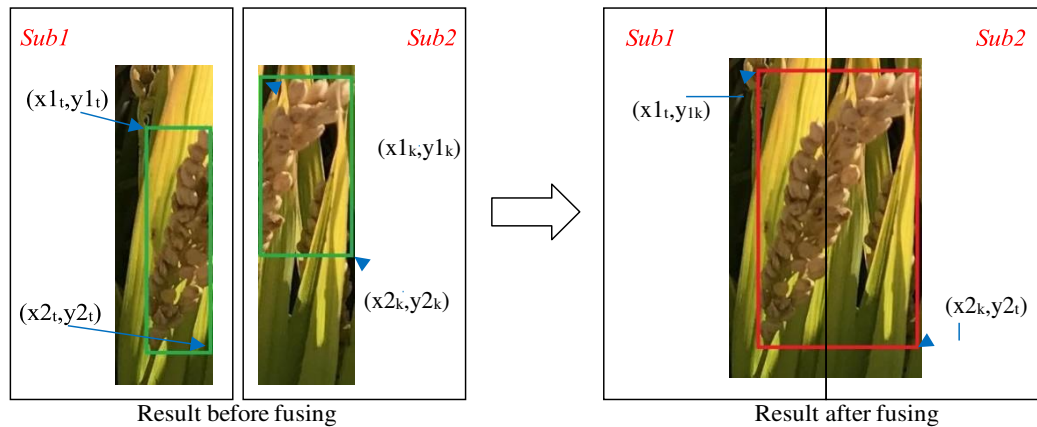


Fig. 3 Illustrated the fusion of vertically dissected rice panicles

## 220 3 Construction of dataset and model

### 221 3.1 Image data acquisition

222 The rice variety chosen is ‘Nanjing46’ and all images were acquired in Nanjing,  
 223 Jiangsu Province, China. The field consisted of a widely cultivated rice variety with  
 224 planting scheme of 3-5 seedlings per hole and 30×12 cm spacing between plants. The  
 225 imaging was performed using random viewing angles at objective distances of ~60  
 226 cm towards the rice plant using a Canon EOS 70D camera with resolutions of  
 227 4032×3024 pixels. The images contain various numbers of small-sized panicles  
 228 ranging from 50-90 per image, which have shown the complex interaction  
 229 relationship between different rice plants. As shown in Figure 4, there were 141  
 230 images and 126 images acquired under normal (9:00 am) and strong (2:00 pm)  
 231 illumination conditions respectively. The picture of the rice panicle appears in yellow  
 232 color, and the full image is filled with large number of light greenish rice leaves  
 233 together with shadows due to the oblique illumination angle and partially due to the  
 234 leaf occlusions. The average dimensions (length × width) of panicles in the image

235 data is about  $260 \times 180$  pixels after selecting 200 independent panicles randomly and  
236 calculating the average size (length  $\times$  width) of their minimum circumscribed  
237 rectangles.

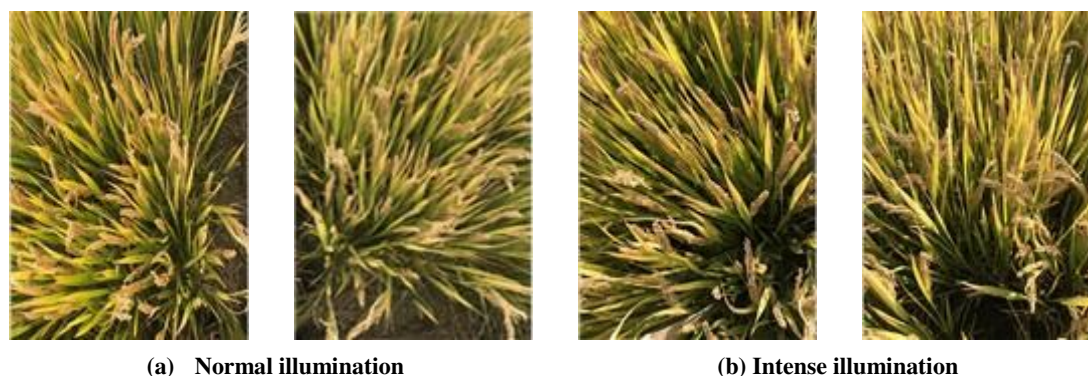


Fig. 4 Sample of have been taken under different viewing angles and illumination conditions

## 238 3.2 Multi-scale hybrid window dataset construction

### 239 3.2.1 Calculate the structure of the MHW

240 The average size of rice panicle in the data set is about  $260 \times 180$  pixels which is  
241 less than one-tenth of the image size with occupancy about 0.4% of the full picture.  
242 This gives the most appropriate dimensions of the input images ranging between  
243  $260 \times 180$  pixels and  $2600 \times 1800$  pixels as according to equation 4. As mentioned in  
244 section 2.2.1, the VGG16 network has been chosen because it is more effective to  
245 learn the features of objects particularly those with physical dimensions like that in  
246 our data set. The optimal dimensions of each layer of the multi-scale hybrid window  
247 can be assessed through equation 5, which gives the topmost 3 layers to be ideally  
248 having  $2016 \times 1512$  pixels,  $1008 \times 756$  pixels and  $504 \times 378$  pixels respectively.  
249 Although theoretically the more of the network layers the richer that the features can  
250 be learned, however, it is a balance between performance and computational



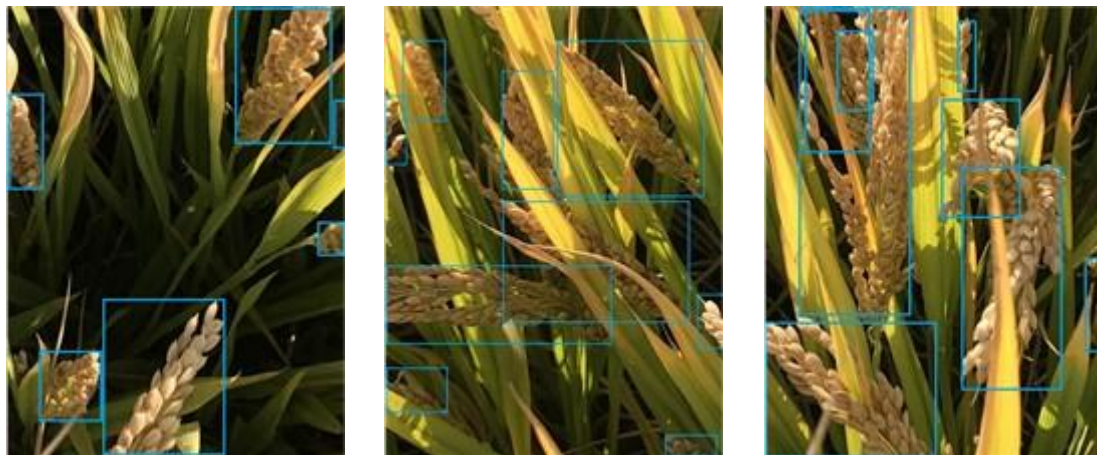
251 complexity. When the layer with input images of sizes  $504 \times 378$  pixels, it contains  
252 utmost only a few rice panicles which may not be economical in view of the amount  
253 of the extra computational and labeling workload involved. Hence, only the two extra  
254 topmost layers have been utilized in this work.

### 255 **3.2.2 Formation of the MHW dataset**

256 Among the 267 rice pictures collected, 130 of those (~50%) were randomly  
257 selected as the training set, and 57 pictures (~20%) were used as the validation set and  
258 the remaining 80 pictures (~30%) was used as the test data set. There is no data  
259 overlap among the training, validation and test sets. For the model training, we only  
260 construct the MHW dataset for the training set and the validation set. Conventional  
261 subsampling using a fixed scheme for altering image dimensions (Ghiasi et al., 2016)  
262 may not be desirable when the problem in question consists of targets in various sizes.  
263 Here, for each image in the training and validation data set, the raw image at  
264  $4032 \times 3024$  pixels resolution (hereafter referred as R1) is divided along the length and  
265 width in 4 and 2 equal parts respectively to form a four and sixteen units of sub-  
266 images respectively. Then these 4 sub-images at  $2016 \times 1512$  pixels resolution  
267 (hereafter referred as R2), and 16 at  $1008 \times 756$  pixels resolution (hereafter referred as  
268 R3) together with the raw image are collectively termed as multi-scale hybrid  
269 windows (MHW). Alternative MHW partition schemes which select different layers  
270 to train the model (such as R1 & R2, R2 & R3) have also been utilized in the  
271 experiment.

### 272 3.2.3 Target labeling schemes

273 The labeling of MHW images for training and validation dataset has been  
274 performed manually by recording the coordinates of the minimum circumscribed  
275 rectangle of the panicle, using the annotation software named 'LabelImg'. In the case  
276 of panicles that have been partitioned into several parts, all parts are labeled as  
277 independent rice panicles. In the case of the rice panicles that are occluded by leaves,  
278 only the exposed parts are labeled as independent panicles. For panicles that are  
279 overlapping to each other, the front panicles are labeled as independent target while  
280 the rear part will be marked only if they are visible. Figure 5 shows some examples of  
281 annotation schemes that have been adopted in this work.



(a) Independent panicles

(b) Panicles covered by leaves

(c) Overlapping panicles

Fig. 5 Examples of manual annotations of panicles

### 282 3.3 Configuration of test dataset for experiments

283 The remaining 80 raw pictures at resolution of 4032×3024 pixels (i.e. at 'R1') in  
284 the section 3.2.2 was termed as the 'Dataset\_test' in this paper. Each image in the  
285 Dataset\_test was then partitioned equally into 16 sub-images giving a total of 1280  
286 pictures at 1008×756 pixels (i.e. at 'R3'), which is collectively referred as

287 ‘Dataset\_test\_1’. The number of panicles in the picture of Dataset\_test\_1 ranges from  
 288 0-20. By merging two of the adjacent neighboring sub-images of the 16 partitioned  
 289 images of the raw pictures produces  $4 \times 80$  of new images at resolution of  $2016 \times 1512$   
 290 (i.e. at ‘R2’). All these sub-images were then sorted into another two data sets  
 291 (Dataset\_test\_2 and Dataset\_test\_3) as according to the number of panicles in the  
 292 imagery as illustrated in Table 3. These 3 data sets provide a range of different  
 293 number (and hence different sizes) of panicles as targets for the classifiers to detect  
 294 (and count) under various degrees of background cluttering.

295 Images of rice panicles collected in real fields are normally exhibit blurring and  
 296 discoloring due to the complicated environment in the rice field. Imaging such  
 297 complex scene by using limited depth of view optical systems under various  
 298 illumination geometries, will result in some objects that are out-of-focus and/or  
 299 discolored due to the variable irradiance and also targets at various depth across the  
 300 scene. As mentioned image data had been collected at two different solar irradiances:  
 301 one at 9 am (thereafter referred as ‘normal’ illumination) and also at 2 pm (thereafter  
 302 referred as ‘intense’ illumination). Another data set, termed as the ‘Dataset\_test\_4’  
 303 which is organized in four categories of a) in-focus & normal illumination, b) in-focus  
 304 & intense illumination, c) blurry & normal illumination and d) blurry & intense  
 305 illumination.

306 **Table 3. Description of the datasets that have been employed in this study**

Name of the Datasets	Composition of Dataset		
	Category	Size of Image Pictures in Dataset	Number of Pictures in Dataset

Dataset_test	Original test images	4032×3024	80
Dataset_test_1	Cut in 16 equal parts	1008×756	1280
Dataset_test_2	0~10(panicle number in sub-window image)	1008×756	205
	11~20(panicle number in sub-window image)	1008×756	108
	21~30(panicle number in sub-window image)	1008×1512	70
	31~40(panicle number in sub-window image)	1008×1512	41
Dataset_test_3	41~50(panicle number in image)	4032×3024	22
	51~60(panicle number in image)	4032×3024	22
	61~70(panicle number in image)	4032×3024	16
	71~80(panicle number in image)	4032×3024	9
	81~90(panicle number in image)	4032×3024	7
Dataset_test_4	In-focused & Normal illumination	1008×756	67
	In-focused & Intense illumination	1008×756	72
	Blurry & Normal illumination	1008×756	62
	Blurry & Intense illumination	1008×756	74

### 307 3.4 Construct the automatic rice panicle counting model

#### 308 3.4.1 Computational hardware and platform

309 All processing performed in this work was carried out by the AMAX's PSC-  
310 HB1X deep learning workstation which consisted of an Intel(R) E5-2600 v3 CPU  
311 with clock speed of 2.1GHZ, 128GB DRAM, 1TB hard disk and with a GeForce  
312 GTX Titan X graphics card. The operating environment was Ubuntu 16.0.4, Caffe,  
313 Python 2.7.

#### 314 3.4.2 Model training

315 The proposed MHW-PD network consists of three parts: the feature learning  
316 network, the candidate region generation network and the detection network (Figure  
317 6). The feature learning network utilizes the VGG16 network but without its  
318 classification layer. The region generation network traverses the feature map  
319 (stride=1) with a 3×3 convolution kernel and a 9 candidate region with three aspect  
320 ratios of 1:1, 2:1 and 1:2 to indicate the high probability of target (panicle) presence is

321 generated by the proposal layer. The detection network uses a convolution operation  
 322 with a convolution kernel size of 1x1 and a sliding step size of 1 to achieve full  
 323 connectivity.

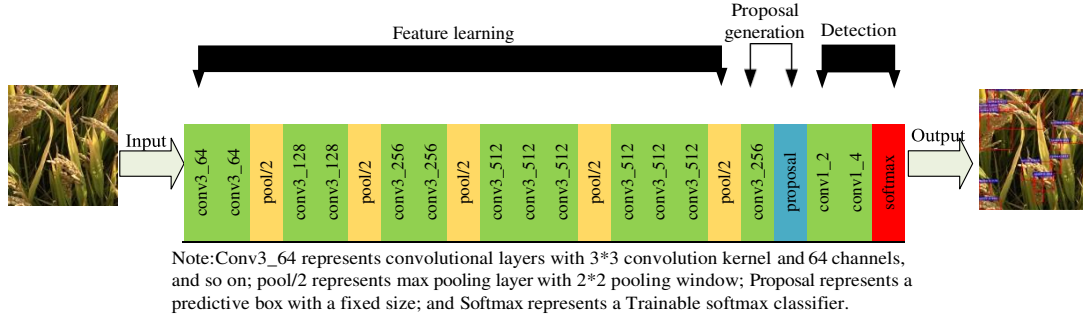


**Fig. 6 Schematic Structural configuration of the proposed MHW-PD network**

324 The VGG16 network is trained through the optimization of the loss function  
 325 using the stochastic gradient descent (SGD) method for the identification of panicles,  
 326 and the location of the targets are obtained through the regression model. We set the  
 327 batch-size and iteration steps to 128 and 80000 respectively, and the learning rate  
 328 changes from 0.001 to 0.0001 after iteration steps reaches 50000. The loss function  
 329 consists of contributions from the classification and regression loss as shown in  
 330 equation (6):

$$331 \quad (\{P\}, \{t\}) = \frac{1}{N_{cls}} \sum_i L_i (i, *) + \lambda \frac{1}{N_{reg}} \sum_i P_i^* L_i (t, t^*) \quad (6)$$

332 Where the  $N_{cls}$  represents the mini-batch size of training,  $N_{reg}$  represents the  
 333 generated number of candidate regions,  $i$  is the anchor number, the weighting  
 334 parameter  $\lambda$  is set as  $\lambda=10$ . The  $P_i$  is the probability of the anchor point being as  
 335 target, and when the anchor point is predicted as positive the corresponding  $P_i^*$   
 336 value is given as 1 and otherwise it is 0 if the anchor is negative.  $t_i$  and  $t_i^*$   
 337 represent the coordinates of the upper left and lower right vertex of the predicted

338 bouncing box respectively.  $L_{cls}$  and  $L_{reg}$  are the logarithmic and robust regression

339 loss respectively:

$$340 \quad L_{cls}(P_i, P^*) = -\log [P_i^* P_i + (1 - P_i^*)(1 - P_i)] \quad (1)$$

$$341 \quad L_{reg}(t_i, t_i^*) = \begin{cases} 0.5(t_i - t_i^*)^2 & |t_i - t_i^*| < 1 \\ |t_i - t_i^*| - 0.5 & |t_i - t_i^*| \geq 1 \end{cases} \quad (8)$$

### 342 3.5 Performance assessment indexes

343 The counting accuracy and the false detection rate have been utilized as the  
 344 performance indexes in this work. The counting accuracy ( $P_c$ ) refers to the ratio of  
 345 detecting the correct number of panicles to the actual number of panicles; while the  
 346 false detection rate ( $P_e$ ) is the ratio of the detection error (false positive) to the actual  
 347 number of panicles (ground truth) in the imagery data set:

$$348 \quad P_c = N_{cor}/N_{real} \quad (9)$$

$$349 \quad P_e = N_{err}/N_{real} \quad (10)$$

350 Where  $N_{cor}$  and  $N_{err}$  are the correct (true positive) and wrong (false positive)

351 number of panicles detected by the model respectively, and  $N_{real}$  represents the

352 actual number of panicles in the test sample.

353 Prior to the accuracy assessment, the repeated counting of the same panicle from

354 the MHW partitioned pictures is firstly evaluated. This is achieved through the

355 assessment of the repetition ratio ( $P_{rep}$ ) as shown in the equations (11), (12) and (13):

$$356 \quad P_{rep} = \frac{N_{rep}}{\sum^k N} \quad (11)$$

$$357 \quad N_{rep} = \sum^k_{i=1} N_{subi} - N_{cor} \quad (12)$$

$$i = 1$$

$$P_{rrep} = \frac{\sum_{i=1}^k N_{subi} - N_{rep}}{N_{terp}} \quad (13)$$

where  $N_{rep}$  represents the number of the repeated panicles that has been removed by the fusion algorithm;  $N_{subi}$  is number of the detected panicle in the  $i^{th}$  sub-window;  $k$  is the total number of the sub-windows in the picture;  $N_{cor}$  represents the number of panicles detected after image fusion;  $P_{rrep}$  is the de-duplication rate and  $N_{terp}$  is the number of the panicles that have been counted repeatedly.

## 4 Results

### 4.1 Parameters that affect the performances of classifier

Based on the hardware mentioned in section 3.4.1, it cost about 0.102s to test a sub image for our model. In addition, to testify how the performance of the classifier is affected by the receptive field of the network, the number of layers in the hybrid windows and the effectiveness of the proposed MHW image partitioning method, two different ways of sample preparations have been utilized:

A . MHW partitioning method (see section 3.2)

B . Down-sampling method (DS):

a. Each image in the training and validation data sets (i.e. the Dataset\_test) is down-sampled by a factor of 2 from the raw resolution of R1 into R2, which is then down-sampled again into R3. The down sampling was done through Laplacian filtering method (Ghiasi et al., 2016).

b. This method does not exploit any window partitioning.

The experiment was performed using one to three layers of the MHW, two



379 different networks (ZF and VGG16) which had receptive fields to target size ratio ( $S_{RF}$   
380  $/S_{obj}$ ) of 0.4 and 0.96 respectively (see Table 1), and data prepared with (i.e. the  
381 MHW method) and without window partitioning processing (i.e. the DS method). The  
382 averaged counting accuracy  $P_c$  over 3 experimental runs using pictures of  
383 dataset\_test\_1 is shown in Table 4.

**384** **Table 4. Average panicle detection results under various network configurations**

Number of MHW layers	Resolution of MHW layer	$P_c$ % (Average $\pm$ STD)			
		Down sampling (DS)		MHW	
		ZF	VGG16	ZF	VGG16
1	4032×3024	31.0% $\pm$ 0.37%	34.7% $\pm$ 0.37%	37.4% $\pm$ 1.12%	38.1% $\pm$ 0.56%
1	2016×1512	38.7% $\pm$ 0.96%	42.3% $\pm$ 0.37%	45.2% $\pm$ 0.37%	47.7% $\pm$ 0.56%
1	1008×756	50.2% $\pm$ 0.55%	53.5% $\pm$ 0.56%	58.4% $\pm$ 0.37%	61.2% $\pm$ 0.56%
2	4032×3024	41.6% $\pm$ 1.10%	44.7% $\pm$ 1.12%	47.9% $\pm$ 0.56%	50.2% $\pm$ 0.55%
2	2016×1512	53.5% $\pm$ 0.56%	56.5% $\pm$ 1.17%	63.0% $\pm$ 0.92%	66.7% $\pm$ 0.56%
2	1008×756	63.5% $\pm$ 0.73%	72.9% $\pm$ 0.92%	73.1% $\pm$ 0.76%	78.1% $\pm$ 0.73%
3	4032×3024	74.8% $\pm$ 0.37%	78.5% $\pm$ 0.36%	83.3% $\pm$ 0.92%	87.2% $\pm$ 0.37%
	2016×1512				
	1008×756				

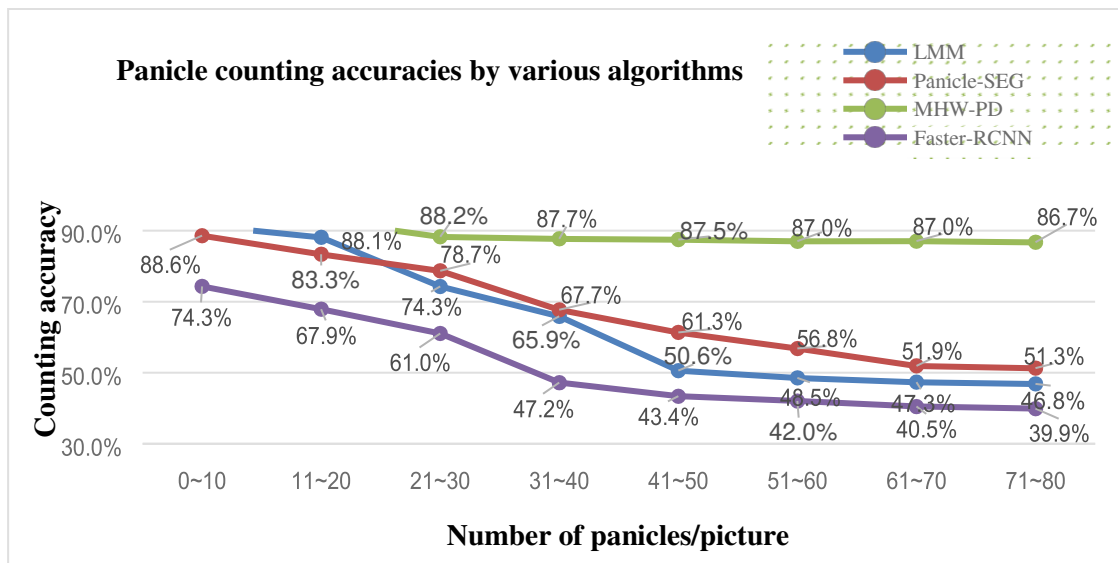
385 Firstly, it is noted that the reduction of the layer resolution from R1 (4032×3024  
386 pixels) to R3 (1008×756 pixels), e.g. when the single layer of MHW of the VGG16  
387 network is used, the panicle counting accuracy is increased from 38.1% to 61.2%.  
388 This is an almost 60% better detection when the layer is in lower (i.e. at R3)  
389 resolution. This trend of enhancement in panicle counting accuracy is seen regardless  
390 whether the data set was prepared with or without window partitioning. Secondly, the  
391 detection performance by the VGG16 network is ~5% better than that of the ZF  
392 network. This apparent small difference observed from the well matched receptive

393 field of the VGG16 comparing to the very mismatched ZF network, is mainly due to  
394 the mixture of panicle densities in the current employed dataset\_test\_1. The proposed  
395 MHW enhances more of detection accuracy when the target sizes are small, i.e. when  
396 the densities of panicles are high (see section 4.2). Thirdly, when the image  
397 partitioning technique is applied (i.e. the MHW method) there is 14.4% increase in the  
398 counting accuracy in comparison to the detection that performed using non-image  
399 partitioning technique (i.e. the DS method). This can be seen, e.g. from the 61.2%  
400 accuracy given by the single layer of MHW of the VGG16 that uses input data at R3  
401 resolution, in direct comparison to that of 53.5% obtained from the down-sampling  
402 (DS) method. Note that this ~14% of performance enhancement by using MHW is not  
403 a representative figure because of the mixed panicle densities in the dataset\_test\_1  
404 that has been employed in this experiment. Fourthly, it is well-known that the  
405 increasing number of the MWH layers improves the detection performance in general,  
406 which can be seen from Table 4 that there is over 40% increase of panicle counting  
407 accuracy when the number of layers is increased from 1 to 3. Despite of using the  
408 image data set (i.e. the dataset\_test\_1) that contains a mixture of different panicle  
409 densities, the results presented in this section indicate that the use of multi-scale  
410 hybrid windows enhances the feature learning capacity of the network, particularly  
411 when the target sizes in the imagery is closely match to the receptive field of the  
412 feature extraction network.

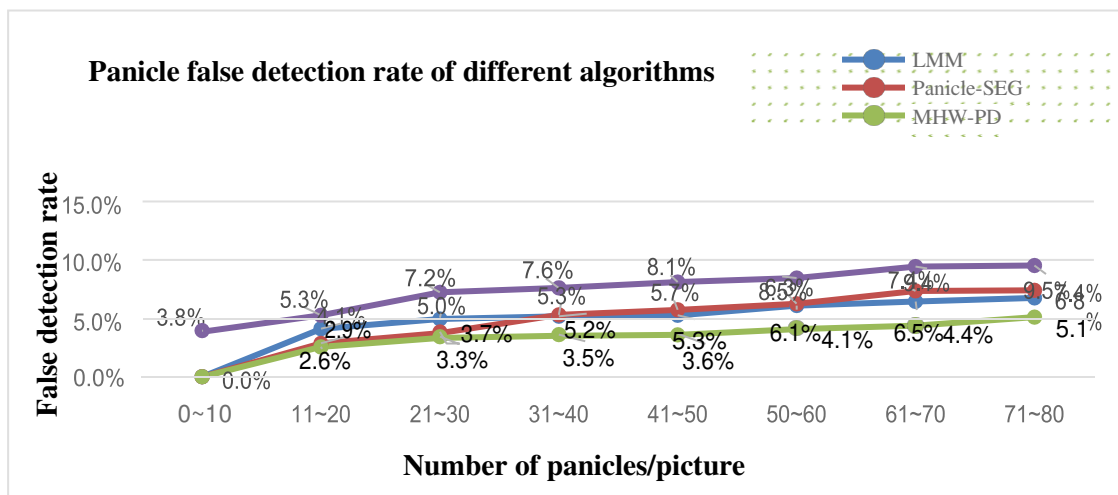
## 413 4.2 Effectiveness of MHW-PD for the detection of large number of panicles

414 Followed by the positive results given by the previous section, the experiment  
415 here is aimed at assessing how effective is the proposed MHW-PD for the  
416 identification of different number (i.e. density) of rice panicles of the scene which is  
417 presented by the input imagery data. This section examines the proposed method  
418 vigorously by assessing the ability of the proposed MHW-PD method for counting  
419 high number of panicles (i.e. small target size), and, to compare its performance with  
420 respected to various existing algorithms. Three competing methods: a) the technique  
421 that based upon filtering using Laplacian, Median and Maxima (LMM)  
422 filters(Fernandez-Gallego et al., 2018); b) the Panicle-Seg(Xiong et al., 2017) which  
423 segments rice panicles (i.e. identification) using super-pixel clustering and CNN  
424 classification and c) the Faster-RCNN that performs panicles detection without any  
425 window partitions; had been utilized here to verify the usefulness of the proposed  
426 MHW technique for enhancing the extraction of features particularly those from small  
427 targets. Both Dataset\_test\_2 and Dataset\_test\_3 had been used as the test data for all  
428 classifiers employed in this experiment. All competing classifiers had been trained  
429 using the 130 pictures of the training data set which were in R1 resolution (i.e.  
430 4032×3024 pixels), while the proposed MHW-PD was trained using the partitioned  
431 images in 3 different scales as described in section 4.4.1. All experiments were based  
432 on the VGG16 and they were repeated 3 times. The abilities in terms of the averaged  
433 counting accuracies and error detection rates of all classifiers to cope with scenes (i.e.

434 images) which contain various numbers of panicles are plotted in Figure 7.



(a) The Counting accuracy of the MHW-PD and together with other competing algorithms as a function of number of panicle/picture



(b) The false detection rate of the MHW-PD and the other competing algorithms as a function of number of panicle/picture

**Fig. 7** The Detection results of the MHW-PD and together with other competing algorithms to demonstrate the effectiveness of the proposed method particularly when high numbers of panicles are present in the scene

435 Figure 7 displays a rather astonished picture which exhibits the robustness of the  
 436 classifiers to the increasing complexity of the rice field conditions vividly. At a glance  
 437 there are two rather distinct trends that can be observed: one is the rapid decreasing  
 438 detection performance, in the order of ~40%, when the number of panicles is

439 increased from ~10 to ~50 in the scene. The other obvious trend is the very robust  
440 detection performance, with a slight drop of ~8% even when the panicle number in  
441 the scene is increased to 70-80/picture. The latter result is given by the proposed  
442 MHW-PD method which utilizes a pre-processing technique with the classification  
443 unit invariant to other competing methods (e.g. the Faster-RCNN).

444 One point to note is the direct comparison between the performances of the  
445 proposed MHW-PD with respected to the Faster-RCNN: in both cases the processing  
446 networks are essentially the same, however, the panicle classification performances  
447 between these two seemingly the same network are completely different. The  
448 averaged detection accuracies given by the Faster-RCNN and the MHW-PD for the  
449 scenes with panicle number <40 (i.e. when the target sizes are much larger than  
450 260×180 pixels) are 62.6% and 90.8% respectively. This is almost 45% better  
451 detection by the MHW-PD when the panicle sizes are relatively large. However, the  
452 same two techniques for classifying the scenes with panicle number between 40 and  
453 80 give the averaged accuracies of 41% and 87% respectively. This is over 110% of  
454 better detection by the proposed MHW-PD when the panicle sizes are small (i.e.  
455 smaller than the average size of 260×180 pixels).

456 Figure 8 depicts representative classified images of the rice panicle scenes  
457 obtained by using the proposed MHW-PD method. The wide range of target sizes, as  
458 depicted by the huge variations of areas of the bounding boxes from large in Figure  
459 8(a) to very small in Figure 8(e), highlights the increasing complexity of the scene

460 which induces higher clutter background and the increasing difficulties to extract the  
461 feature of small targets faithfully as that depicted in Figure 8(d) & (e). This result may  
462 give another evidence that the detection capability of the propose MHW-PD method  
463 is robust against high number (density) of panicles in the rice field.

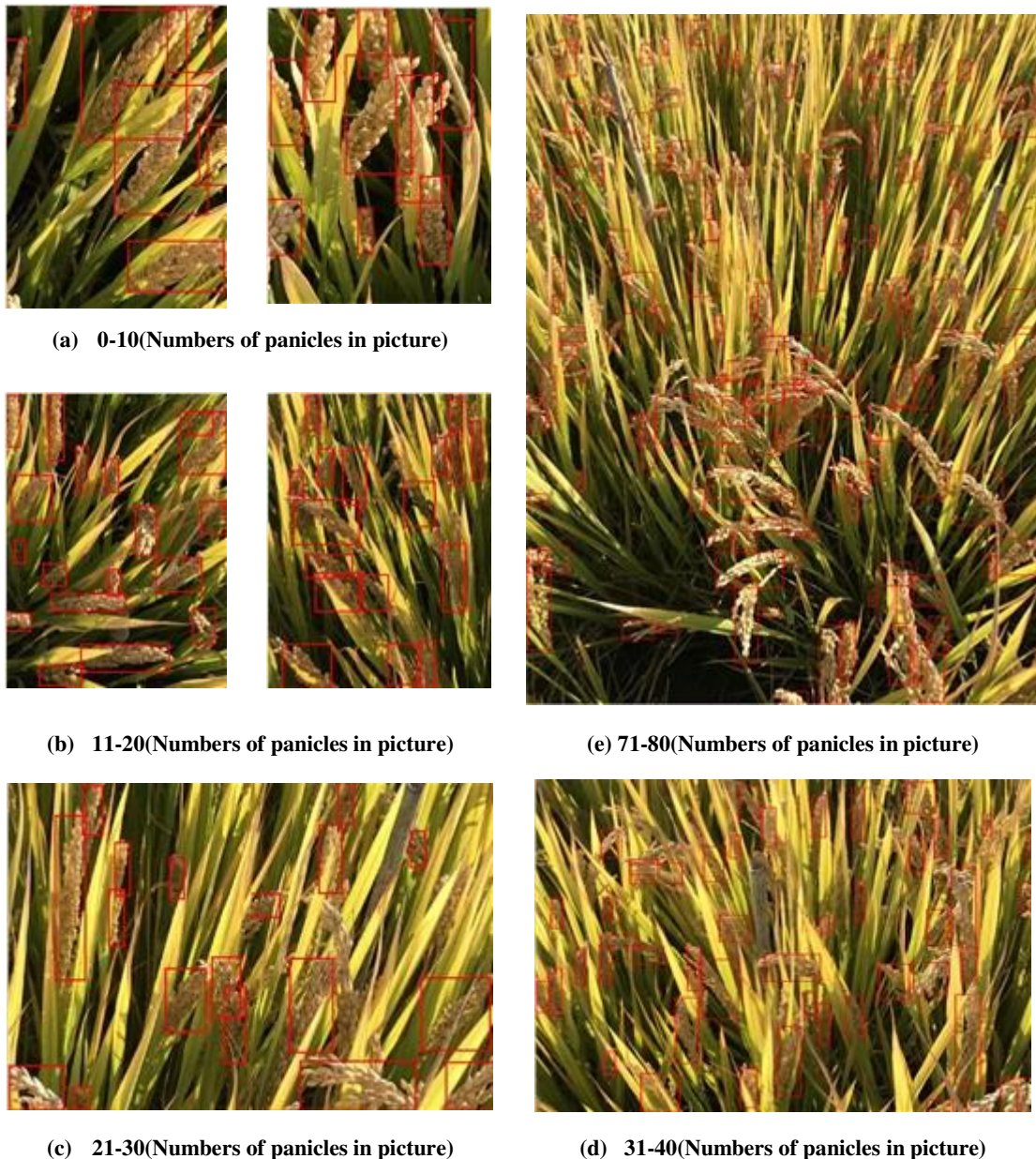


Fig. 8 Sample of pictures to illustrate the effectiveness of the proposed MHW-PD for the detection of various sizes of panicles in the scene

#### 464 4. 3 Robustness of MHW-PD against numbers of panicles in the scene

465 This section highlights how the proposed MHW-PD enhances the detection of

466 small target in the imagery data over the conventional classification routine. Here, the  
467 ‘small’ target in this work is referred to the relative size (in pixel unit) of the target  
468 object with respected to the pixel dimension of the input images. Figure 9a illustrates  
469 the typical classification result produced by the classifier (Faster-RCNN) in which the  
470 dimension of the input test image is at R1 resolution (i.e. 4032×3024 pixels). It is seen  
471 that some small panicles have been missed out in this classification result. The  
472 classification of the same test image after it is partitioned into 4 sub-windows (at R3  
473 resolution) exhibits much better detections as it is illustrated in Figure 9b. After the  
474 removal of duplicated counts of dissected panicles at the boundary of sub-windows  
475 through the fusion algorithm, the end result as depicted in Figure 9c shows much  
476 better detection than that of Figure 9a. At a glance over Figure 9a and Figure 9c, one  
477 may notice immediately the distinct difference of the sizes of the panicle bounding  
478 boxes between these two figures: more small bounding boxes can be spotted from the  
479 MHW-PD result (Figure 9c).



(a) Result without cutting

(b) Results of HW after cutting

(c) Result after fusing

**Fig. 9 Demonstrate the effectiveness of the MHW-PD system**

480 Since the sub-window fusion plays an essential part in the overall performance of  
 481 the MHW-PD, the robustness of the fusion algorithm over increasing complexity of  
 482 the scene was investigated here. The experiment was designed to evaluate the  
 483 detection performance of the algorithm for a range of assorted number of panicles in  
 484 the data set (Dataset\_test\_3). The repetition ratio ( $P_{rep}$ ) is to measure the probability  
 485 of panicles being counted repeatedly, while the de-duplication rate ( $P_{rrep}$ ) represents  
 486 the ability of the fusion algorithm to remove the repeated counts. It can be seen from  
 487 Figure 10 that  $P_{rep}$  is rather constant in the medium density (number) of panicles  
 488 and it increases slightly at high number of targets in the scene. The  $P_{rrep}$  also  
 489 exhibits rather steady performance at ~95% removal rate when the panicle number  
 490 <90, but it tends to decrease slightly to ~92% at high end of >100 panicles in the  
 491 scene. This result may give another support towards the robustness of the proposed  
 492 MHW-PD system.

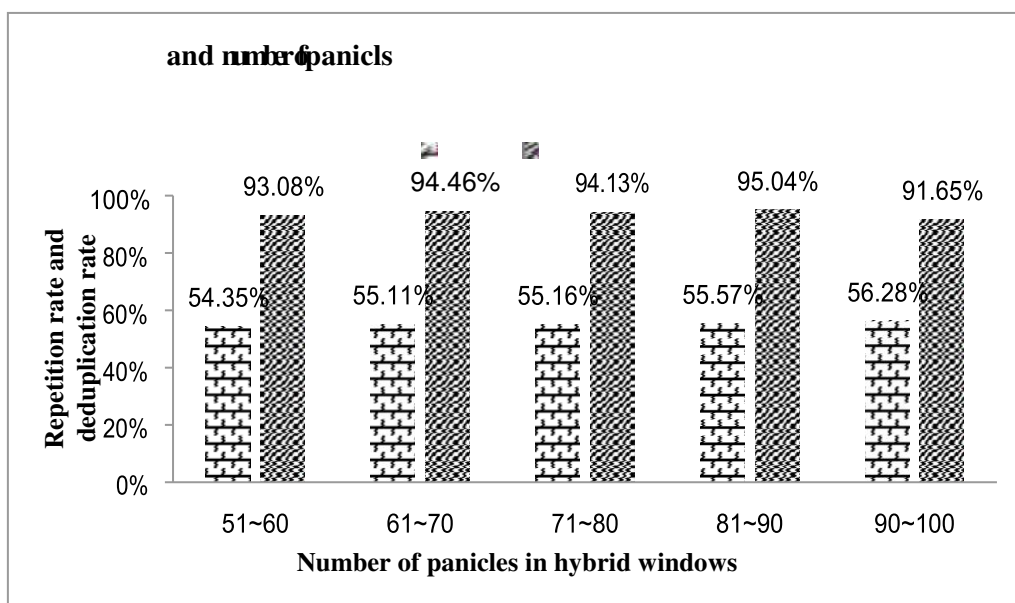


Fig. 10 Highlight the robustness of the  $P_{rep}$  and  $P_{rrep}$  of the MHW-PD against the number of panicles



#### 493 4. 4 Robustness of MHW-PD against illumination and imaging artefacts

494 As shown in figure 8(e), it is observed that the detection results in the top of this  
495 image are obviously worsen than the bottom part. During the course of this work, we  
496 found that the bottom of images were sharp (in-focused) while the top part were  
497 blurry and fuzzy. To understand the robustness of our counting model when the  
498 quality of the input images was subjected to various degree of blurriness and  
499 shadowing artefacts, the Dataset\_test\_4 had been used as the test data (see Table 3),  
500 which consisted of field images subjected to various degree of blurriness and  
501 shadowing and taken under normal (i.e. weak shadowing) and intense (i.e. strong  
502 shadowing) illumination conditions. The number of panicles per picture in the  
503 Dataset\_test\_4 was <20. The experiments were run 3 times based on VGG16 to  
504 obtain the mean detectio2n accuracy and the associated standard deviation errors.  
505 Typical images of the classification outputs from the MHW-PD for the detection of  
506 panicles from the dataset\_test\_4 which contains blurry and strong shadowing pictures  
507 are shown in Figure 11. The average counting accuracies and the average false  
508 detection rates for the panicle detections of this data set are tabulated in Table 5,  
509 which reveals that the hard shadowing imposed by the intense illumination does not  
510 affect the detection efficiency significantly. However, there is ~24% drop of detection  
511 when the input images for testing are blurry. This may indicate that the fuzziness of  
512 the input image does affect the extraction of textural features as expected.

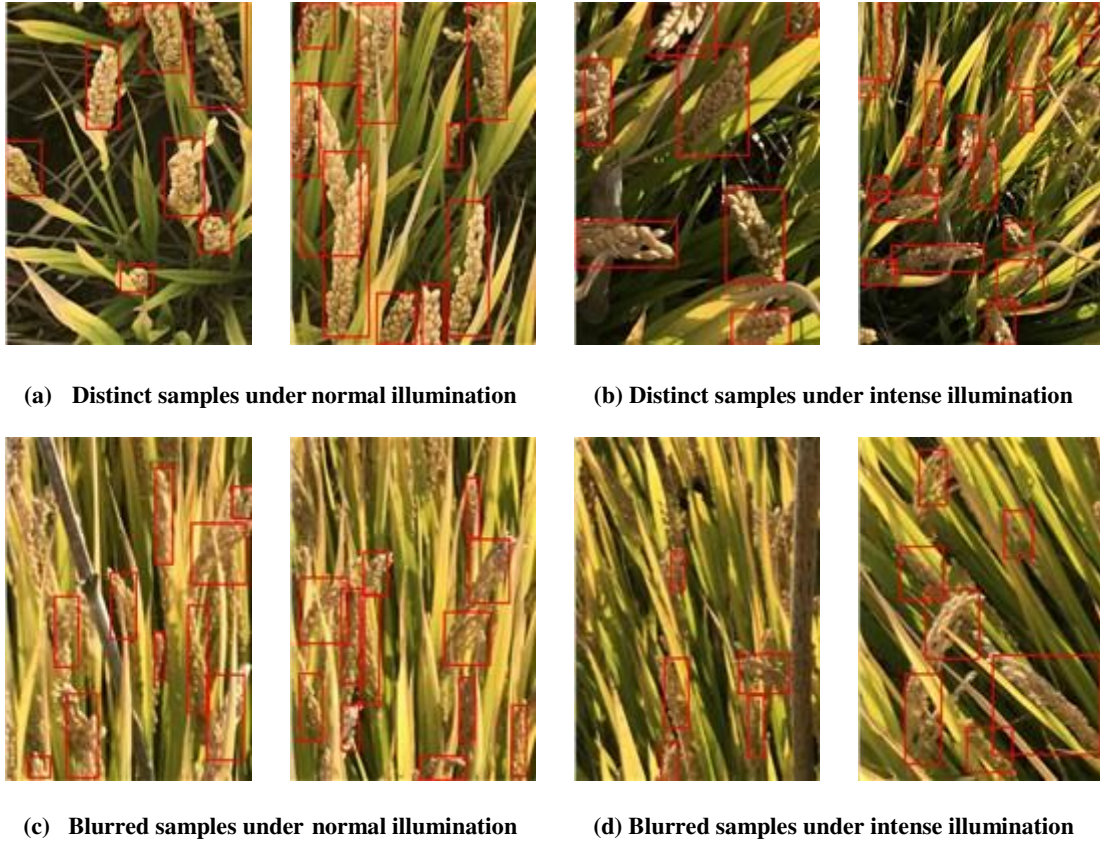


Fig. 11 To illustrate the Detection of panicles under various illumination and imaging conditions

513

Table 5. Average detection accuracies for images taken under various illumination and imaging conditions

Quality of input image data	Illumination conditions	$P_d/\%$ (Average $\pm$ SID)	$P_e/\%$ (Average $\pm$ STD)
In-focused pictures	Normal (weak) illumination	94.5% $\pm$ 0.78%	1.6% $\pm$ 0.26%
	Intense (strong) illumination	92.4% $\pm$ 0.37%	2.0% $\pm$ 0.16%
	Mixture of Normal & Intense illumination	93.4% $\pm$ 0.51%	1.8% $\pm$ 0.07%
Blurry pictures	Normal (weak) illumination	70.1% $\pm$ 0.89%	3.3% $\pm$ 0.42%
	Intense (strong) illumination	68.5% $\pm$ 1.08%	3.5% $\pm$ 0.34%
	Mixture of Normal & Intense illumination	69.3% $\pm$ 0.46%	3.4% $\pm$ 0.27%

## 514 5 Discussions

515 This work has reported a method (MHW-PD) to count the in-field small-sized  
516 rice panicle and function robustly independent of the panicle density. Based on the  
517 results given by the series of experiments, it is suggested that the dynamic strategies  
518 for network selection multi-scale hybrid windows construction tend to enhance the

519 feature learning capacity of the small-sized panicles and eliminate the impact of the  
520 increase in the number of rice panicles. Compared to the pure counting method based  
521 on thermal imagery (Fernandez et al., 2019), it should be noted that, the individual  
522 rice panicle images can be segmented easily since their positions are predicted by  
523 MHW-PD. It means more phenotypic traits can be analyzed further in detail, such as  
524 the length of panicle, the radian of panicle, the number of panicle grains, the disease  
525 spot or the saturation of panicle grains and so on. In addition, the result of 87% is an  
526 average accuracy of different clarities, illuminations, occlusions and panicle numbers  
527 per image. While most of the current phenotypic studies focus on indoor potted rice,  
528 which means more stable imaging conditions (no fuzzy panicles), fewer panicles and  
529 less occlusion in the image. Thus, we suppose the MHW-PD can meet the needs of  
530 phenotypic researchers to some extent for mining the relationship from traits to  
531 genotypes, while there are also some limitations and practical issues we have to  
532 consider when the MHW-PD applied in real situations, which may constitute research  
533 directions that will be pursued in the future work.

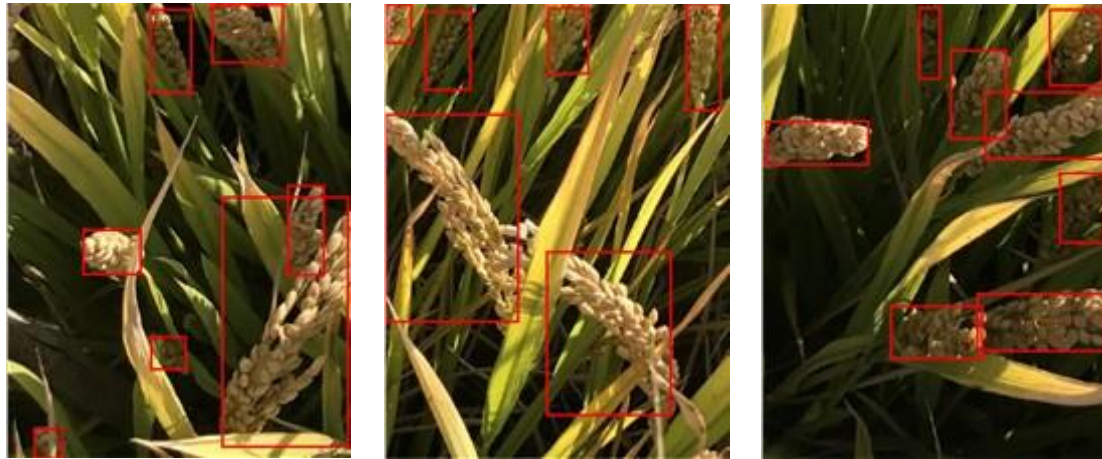
534 **(1) MHW-PD against occlusions.** Occlusion has been one of the main factors that  
535 affect the performance of panicle counting, which may come from the high plant  
536 density and drooping, particularly when the assessment method is based on image  
537 recognition technology. In this section, 3 different kinds of occlusions have been  
538 studied: a) independent panicle when there is no obstruction, b) occlusion by leaf and  
539 c) overlapping panicles. The data set that been utilized in this experiment consisted of

540 <20 panicles/picture and the training/testing conditions of the MHW-PD network  
541 were the same as the previous experiments. Sample pictures of detection results for  
542 the identification of panicles in the data set that consists of these 3 types of occlusions  
543 are shown in Figure 12, and their averaged detection accuracies are tabulated in table  
544 6. The result has shown quite clear that the detection is strongly affected by  
545 occlusions which causes some ~30% degradation of panicle accuracies with respected  
546 to the unobstructed base line, when the target panicle is occluded by leaves. Worse  
547 still is a ~60% drop in the detection accuracy when panicles in the scene are self-  
548 occluded. This large drop in detection efficiency is the inability of the classifier to  
549 discriminate the overlapped panicles and in most cases, it misclassifies the  
550 agglomerated entity as one panicle (see Figure 12b). The occlusion by leaves is not as  
551 severe as that of the self-occlusion as long as the panicle sizes are relatively larger  
552 than the leaf blades. However, the detection is seen worse when small panicles are  
553 occluded by the leaves or when large part of the panicles are covered by leaves (see  
554 Figure 12c). The very limited amount of features is not sufficient enough for the  
555 classifier to discriminate the leaf and panicle.

556 **Table 6. Results of images with different occlusions**

Types of Occlusions	$P_d$ %	$P_c$ %
Independent panicles ( 114 images )	95.5%	1.2%
Panicles partially covered by leaves ( 52 images )	62.8%	6.3%
overlapping panicles ( 46 images )	37.8%	29.4%

557



(a) Detect results of independent panicles



(b) Detect results of overlapping panicles



(c) Detect results of panicles covered by leaves

Fig. 12 Illustrate the detection by the MHW-PD for the panicles that are subjected to various occlusions

558 (2) MHW-PD against different imaging heights. Panicle size is the most important  
 559 factor to consider when we designed the MWH-PD. However, when it comes to the  
 560 different imaging heights, the main effect is the change of average panicle size. For

561 example, if the images taken at a higher/lower altitude, the number of panicles will  
562 rise/fall sharply while the panicle size become smaller/bigger in the single image. Our  
563 ideal is selecting feature learning network which can effectively perceive a complete  
564 panicle and constructing the multi-scale hybrid windows which can extract the multi-  
565 scale panicle features. Therefore, in order to ensure the application effect of the  
566 MHW-PD, we have to design different reasonable image acquisition schemes  
567 (viewing angles, depth of field, focusing ability and optical aberrations et al.) for  
568 different particular imaging heights, which can ensure the panicle size is enough to  
569 find a matching feature learning network. At this time, the gap caused by different  
570 heights can be filled easily by selecting suitable network and constructing suitable  
571 MHW. However, we do not mean the MHW-PD can be applied under any heights  
572 because the sizes of the reception fields of the existing network are limited. From this  
573 angle, there may be a possibility to extend MHW-PD from the camera images to the  
574 high-resolution UAV images in theory, but more issues need to deal with to realize  
575 the application. For example, the huge amount of labeling work and some new  
576 processing mechanisms for the blur of panicles caused by the propeller wind when the  
577 UAV flew at a very low altitude.

578 **(3) MHW-PD against different rice varieties.** The shape of panicles has great  
579 influence on detection accuracy, which not only comes from the panicles of different  
580 rice varieties, but also from the panicles of same variety during different growth  
581 periods. In order to realize large-scale promotion application, we have to solve this

582 inevitable problem, while it is very different to construct a universal model. Firstly,  
583 collecting images of all rice varieties/growth periods and labeling them costs a lot of  
584 money and time. Secondly, universal model means we need count and identify the  
585 species at same time. For deep learning networks, the great difficulty to solve this  
586 problem lies in how we can realize the feature representation of several rice varieties,  
587 which have small difference and even some of the difference is only local. The  
588 features can not only represent the rice panicles but also have enough differentiation  
589 to support the effective fine-grained classification for those different subspecies and  
590 varieties of rice. The problem may become even more difficult for the field scenarios  
591 because of the interference of complex field noise. One possible solution we now  
592 have tried is to iteratively build single model for every variety or growth period and  
593 cascade a multi-discrimination model for counting and identifying.

## 594 **6 Conclusions**

595 Counting small-sized rice panicles efficiently and accurately by using image based  
596 technique has been a challenging task. This paper proposes a new, yet simple method  
597 termed as MHW-PD to realize the efficacy of rice panicle counting especially when  
598 high number (density) of small-sized rice panicles is involved. The main contribution  
599 of this work is to introduce a multi-scale hybrid window (MHW) pre-processing 600  
technique for enhancing the richness of the target feature, and then to maximize the 601 feature  
extraction efficiency of the network through matching the target sizes with the 602 receptive  
field of the network. Through experimental design and result analysis, the

603 conclusions can be summarized as follows:

604 (1) The proposed MHW-PD can significantly improve the counting accuracy for the 605  
scene where large numbers of panicles in a signal image. The combined effects of  
606 selecting the appropriate feature learning network and constructing the optimal 607  
hybrid window shown that the average counting accuracy of MHW-PD is 87.2%,  
608 which achieves >110% of detection efficiency better than that of the Faster- 609  
RCNN for the dense scenes whose number of panicles is between 50 and 80 per 610  
image.

611 (2) The MHW-PD has better stability in counting accuracy for the increasing number 612  
of panicle. When the panicle number increases from 10 to 80, the counting 613  
accuracy of MHW-PD comes down by 7.6%.

614 (3) The proposed MHW-PD can be used for infield scenes with hard shadowing 615  
imposed by intensified illumination, while the imaging and occlusion artefacts 616  
will affect the detection efficiency significantly. There is ~24% drop of detection  
617 when the input images for testing are blurry. When the panicles occluded by 618  
leaves and self-occluded with panicles crossing each other, the counting accuracy  
619 is ~30% and ~60% degradation respected to the unobstructed base line.

## 620 **Acknowledgements**

621 This paper is supported in part by the National Natural Science Foundation of 622  
China (No. 31872847); the Key Program of Science and Technology Infrastructure of 623  
Jiangsu Province of China (Modern Agriculture, BE2019383).



## 624 REFERENCES

625 Aich S, Stavness I. Leaf counting with deep convolutional and deconvolutional 626  
networks. In: Proceedings of the IEEE International Conference on Computer Vision, 627  
2017, pp. 2080-2089.

628 Alkhudaydi T, Zhou J. SpikeletFCN: Counting Spikelets from Infield Wheat Crop 629  
Images Using Fully Convolutional Networks. In: International Conference on 630  
Artificial Intelligence and Soft Computing, 2019, pp. 3-13, Springer.

631 Barré P, Stöver BC, Müller KF, Steinhage V. LeafNet: A computer vision system for 632  
automatic plant species identification. *Ecological Informatics*, 40(2017), pp. 50-56, 633  
10.1016/j.ecoinf.2017.05.005

634 Cointault F, Guerin D, Guillemin JP, Chopinet B. In-field *Triticum aestivum* ear 635  
counting using colour-texture image analysis. *New Zealand Journal of Crop and 636  
Horticultural Science*, 36(2008), pp. 117-130, Doi 10.1080/01140670809510227

637 Dobrescu A, Valerio Giuffrida M, Tsaftaris SA. Leveraging multiple datasets for deep 638  
leaf counting. In: Proceedings of the IEEE International Conference on Computer 639 Vision,  
2017, pp. 2072-2079.

640 Du Y, Cai Y, Tan C, Li Z, Yang G, Feng H, Dong H. Field wheat ears counting based 641  
on superpixel segmentation method. *Scientia Agricultura Sinica*, 52(2019), pp. 21-33, 642  
10.3864/j.issn.0578-1752.2019.01.003

643 Duan LF, Huang CL, Chen GX, Xiong LZ, Liu Q, Yang WN. Determination of rice 644  
panicle numbers during heading by multi-angle imaging. *Crop Journal*, 3(2015), pp.

645 211-219, 10.1016/j.cj.2015.03.002

646 Fernandez-Gallego JA, Kefauver SC, Gutierrez NA, Nieto-Taladriz MT, Araus JL. 647  
Wheat ear counting in-field conditions: high throughput and low-cost approach using 648 RGB  
images. *Plant methods*, 14(2018), pp. 22-34, 10.1186/s13007-018-0289-4

649 Ferrante A, Cartelle J, Savin R, Slafer GA. Yield determination, interplay between 650  
major components and yield stability in a traditional and a contemporary wheat across 651 a  
wide range of environments. *Field Crops Research*, 203(2017), pp. 114-127, 652  
10.1016/j.fcr.2016.12.028

653 Ghiasi G, Fowlkes CC. Laplacian pyramid reconstruction and refinement for semantic 654  
segmentation. In: *European Conference on Computer Vision*, 2016, pp. 519-534, 655  
Springer.

656 Girshick R. Fast r-cnn. In: *Proceedings of the IEEE international conference on 657  
computer vision*, 2015, pp. 1440-1448.

658 Girshick R, Donahue J, Darrell T, Malik J. Rich feature hierarchies for accurate object 659  
detection and semantic segmentation. In: *Proceedings of the IEEE conference on 660  
computer vision and pattern recognition*, 2014, pp. 580-587.

661 Giuffrida MV, Minervini M, Tsafaris SA. Learning to count leaves in rosette plants. 662  
In: *Proceedings of the Computer Vision Problems in Plant Phenotyping (CVPPP)*, 663  
2016, pp. 1.1-1.13.

664 Guo W, Fukatsu T, Ninomiya S. Automated characterization of flowering dynamics 665  
in rice using field-acquired time-series RGB images. *Plant methods*, 11(2015), pp. 7-

666 23, 10.1186/S13007-015-0047-9

667 Han J, Zhang D, Cheng G, Liu N, Xu D. Advanced deep-learning techniques for 668  
salient and category-specific object detection: a survey. *IEEE Signal Processing* 669  
*Magazine*, 35(2018), pp. 84-100, 10.1109/Msp.2017.2749125

670 Hasan MM, Chopin JP, Laga H, Miklavcic SJ. Detection and analysis of wheat spikes 671  
using Convolutional Neural Networks. *Plant methods*, 14(2018), pp. 100-113, 672  
10.1186/S13007-018-0366-8

673 He K, Zhang X, Ren S, Sun J. Spatial pyramid pooling in deep convolutional 674  
networks for visual recognition. *IEEE transactions on pattern analysis and machine* 675  
*intelligence*, 37(2015), pp. 1904-1916, 10.1109/TPAMI.2015.2389824

676 Jin XL, Liu SY, Baret F, Hemerle M, Comar A. Estimates of plant density of wheat 677  
crops at emergence from very low altitude UAV imagery. *Remote Sensing of* 678  
*Environment*, 198(2017), pp. 105-114, 10.1016/j.rse.2017.06.007

679 Krizhevsky A, Sutskever I, Hinton GE. Imagenet classification with deep 680  
convolutional neural networks. In: *Advances in neural information processing* 681  
*systems*, 2012, pp. 1097-1105.

682 Liu W, Anguelov D, Erhan D, Szegedy C, Reed S, Fu C-Y, Berg AC. Ssd: Single shot 683  
multibox detector. In: *European conference on computer vision*, 2016, pp. 21-37, 684  
Springer.

685 Lu H, Cao ZG, Xiao Y, Li YA, Zhu YJ. Region-based colour modelling for joint crop 686  
and maize tassel segmentation. *Biosystems Engineering*, 147(2016), pp. 139-150,

687 10.1016/j.biosystemseng.2016.04.007

688 Madec S, Jin X, Lu H, De Solan B, Liu S, Duyme F, Heritier E, Baret F. Ear density 689  
estimation from high resolution RGB imagery using deep learning technique. 690  
Agricultural and forest meteorology, 264(2019), pp. 225-234,

691 10.1016/j.agrformet.2018.10.013

692 Maldonado Jr W, Barbosa JC. Automatic green fruit counting in orange trees using 693  
digital images. Computers and electronics in agriculture, 127(2016), pp. 572-581, 694  
10.1016/j.compag.2016.07.023

695 Mussadiq Z, Laszlo B, Helyes L, Gyuricza C. Evaluation and comparison of open 696  
source program solutions for automatic seed counting on digital images. Computers 697 and  
electronics in agriculture, 117(2015), pp. 194-199, 10.1016/j.compag.2015.08.010 698

Olsen PA, Ramamurthy KN, Ribera J, Chen Y, Thompson AM, Luss R, Tuinstra M, 699 Abe N.  
Detecting and Counting Panicles in Sorghum Images. In: 2018 IEEE 5th 700 International  
Conference on Data Science and Advanced Analytics (DSAA), 2018, 701 pp. 400-409, IEEE.

702 Pound MP, Atkinson JA, Wells DM, Pridmore TP, French AP. Deep learning for 703  
multi-task plant phenotyping. In: Proceedings of the IEEE International Conference 704 on  
Computer Vision, 2017, pp. 2055-2063.

705 Qiongyan L, Cai J, Berger B, Okamoto M, Miklavcic SJ. Detecting spikes of wheat 706  
plants using neural networks with Laws texture energy. Plant methods, 13(2017), pp. 707 83-  
96, 10.1186/s13007-017-0231-1

708 Redmon J, Divvala S, Girshick R, Farhadi A. You only look once: Unified, real-time 709  
object detection. In: Proceedings of the IEEE conference on computer vision and 710 pattern  
recognition, 2016, pp. 779-788.

711 Redmon J, Farhadi A. YOLO9000: better, faster, stronger. In: Proceedings of the 712  
IEEE conference on computer vision and pattern recognition, 2017, pp. 7263-7271.

713 Ren S, He K, Girshick R, Sun J. Faster r-cnn: Towards real-time object detection with 714  
region proposal networks. In: Advances in neural information processing systems, 715  
2015, pp. 91-99.

716 Simonyan K, Zisserman A. Very deep convolutional networks for large-scale image 717  
recognition. arXiv preprint arXiv:1409.1556, 2014),

718 Slafer GA, Savin R, Sadras VO. Coarse and fine regulation of wheat yield 719  
components in response to genotype and environment. Field Crops Research, 720  
157(2014), pp. 71-83, 10.1016/j.fcr.2013.12.004

721 Stein M, Bargoti S, Underwood J. Image Based Mango Fruit Detection, Localisation 722  
and Yield Estimation Using Multiple View Geometry. Sensors, 16(2016), pp. 1915- 723 1923,  
10.3390/S16111915

724 Szegedy C, Liu W, Jia Y, Sermanet P, Reed S, Anguelov D, Erhan D, Vanhoucke V, 725  
Rabinovich A. Going deeper with convolutions. In: Proceedings of the IEEE 726  
conference on computer vision and pattern recognition, 2015, pp. 1-9.

727 Xiong X, Duan L, Liu L, Tu H, Yang P, Wu D, Chen G, Xiong L, Yang W, Liu Q. 728  
Panicle-SEG: a robust image segmentation method for rice panicles in the field based

729 on deep learning and superpixel optimization. *Plant methods*, 13(2017), pp. 104-119, 730

10.1186/s13007-017-0254-7

731 Zeiler MD, Fergus R. Visualizing and understanding convolutional networks. In: 732  
European conference on computer vision, 2014, pp. 818-833, Springer.

733 Zhou C, Liang D, Yang X, Yang H, Yue J, Yang G. Wheat Ears Counting in Field 734

Conditions Based on Multi-Feature Optimization and TWSVM. *Frontiers in plant 735*

science, 9(2018), pp. 1024-1040, 10.3389/fpls.2018.01024

736

### **Declaration of interests**

The authors declare that they have no known competing financial interests or personal relationships that could have appeared to influence the work reported in this paper.

The authors declare the following financial interests/personal relationships which may be considered as potential competing interests:

None

## CRediT author statement

**Xu can:** Conceptualization, Methodology, Software, Data curation, Writing-Original draft preparation. **Jiang Haiyan:** Formal analysis, Supervision, Writing - Review & Editing, Funding acquisition. **Peter Yuen:** Writing - Review & Editing. **Zaki Ahmad Khan:** Validation Writing - Review & Editing. **Chen Yao:** Validation, Data curation.